Mon. Not. R. Astron. Soc. **000**, 000–000 (0000) Printed 22 August 2016 (MN LATEX style file v2.2)

# Multi-stream portrait of the Cosmic web

Nesar S. Ramachandra, ⋆ Sergei F. Shandarin,
*Department of Physics and Astronomy, University of Kansas, Lawrence, KS 66045*

22 August 2016

arXiv:1412.7768v3 [astro-ph.CO] 19 Aug 2016

**ABSTRACT**

We report the results of the first study of the multi-stream environment of dark matter haloes in cosmological N-body simulations in the ΛCDM cosmology. The full dynamical state of dark matter can be described as a three-dimensional sub-manifold in six-dimensional phase space - the dark matter sheet. In our study we use a Lagrangian sub-manifold $\mathbf{x} = \mathbf{x}(\mathbf{q}, t)$ (where $\mathbf{x}$ and $\mathbf{q}$ are co-moving Eulerian and Lagrangian coordinates respectively), which is dynamically equivalent to the dark matter sheet but is more convenient for numerical analysis. Our major results can be summarized as follows. At the resolution of the simulation i.e. without additional smoothing, the cosmic web represents a hierarchical structure: each halo is embedded in the filamentary framework of the web predominantly at the filament crossings, and each filament is embedded in the wall like fabric of the web at the wall crossings. Locally, each halo or sub-halo is a peak in the number of streams field. The number of streams in the neighbouring filaments is higher than in the neighbouring walls. The walls are regions where number of streams is equal to three or a few. Voids are uniquely defined by the local condition requiring to be a single-stream flow region. The shells of streams around haloes are quite thin and the closest void region is typically within one and a half FOF radius from the center of the halo.

**Key words:** methods: numerical – cosmology: theory – dark matter – large-scale structure of Universe

## 1 INTRODUCTION

The problem of objective identification and quantitative characterization of anisotropic structures in the distribution of galaxies in space emerged after the first evidences of their existence (see the review by Oort 1983 and the references therein). The first theoretical model predicting highly anisotropic concentrations in the mass distribution coming into existence at the non-linear stage of gravitational instability is known as the Zeldovich Approximation (the ZA) (Zel'dovich 1970, for further developments see also Shandarin & Zeldovich 1989 and the references therein). The ZA predicted the formation of 'pancakes' also known as the walls in the currently popular jargon. The later development of the model by Arnold et al. (1982) predicted the formation of filaments along with the pancakes. Klypin & Shandarin (1983) and Shandarin & Klypin (1984) demonstrated that the filaments emerge in the cosmological N-body simulation in three-dimensional space. However, they failed to identify the pancakes at $z = 0$. Both the existence of filaments connecting compact clumps of matter and absence of pancakes were confirmed by Frenk et al. (1983). Puzzled by the absence of the pancakes Klypin & Shandarin (1983) speculated that insufficient mass resolution of the simulation was the cause of the negative outcome. This has been unambiguously confirmed by recent simulations using a better numerical technique of computing a density field from the particle coordinates in cosmological N-body simulations ( Shandarin et al. 2012 and Abel et al. 2012). Klypin & Shandarin 1983 also stressed that the most of filaments are incorporated in 'a single three-dimensional web structure'[1]. They admitted that their simulation did not allow them to confirm the existence of pancakes between the filaments predicted by the ZA (Arnold et al. 1982).

Although the four archetypical elements of the cosmic web: voids, walls/pancakes, filaments and haloes were predicted by ZA and confirmed in cosmological N-body simulation their identification and quantitative characterization remains under vigorous debate (see e.g. Colberg et al. 2008, Elahi et al. 2013, Knebe et al. 2013, Hoffmann et al. 2014). The dark matter haloes are arguably the easiest objects to identify in N-body simulations. They can also be reliably associated with observed objects like galaxies and clusters of galaxies. But even in this case Knebe et al. (2013) refer to almost thirty different halo finders suggested after 2000.

⋆ E-mail: nesar@ku.edu

[1] The term 'cosmic web' was coined by Bond et al. (1996).

© 0000 RAS

Identifying filaments and pancakes/walls is far more controversial in both N-body simulations and galaxy catalogues. For instance, even estimating the global parameters of the web in N-body simulation such as the fractions of volume and mass in voids, walls/pancakes, filaments and haloes produced quite different results. The estimates of volume fractions of voids range from 13 to 86% (Cautun et al. 2014, Falck & Neyrinck 2015, Forero-Romero et al. 2009 , Hahn et al. 2007 , Aragón-Calvo et al. 2010). Similar estimates for walls/pancakes, filaments and haloes are respectively 5-56% 2-26% and 0.1-1%. Estimates of the mass content vary in large ranges as well.

Large differences in the estimates of volume and mass fractions made by different groups are not surprising if we recognize considerable differences in the definitions of the components of the cosmic web and numerical methods used in the estimates. Without trying to provide an exhaustive review of all definitions and techniques used for the quantitative morphological analysis of the web we just briefly describe a few approaches in order to illustrate how different they could be. Some groups study the web morphology using only coordinates of simulation particles, while others use the particle velocities too. Transforming data from point sets to the density and other fields on a grid is also often used because fields allow to use a variety of mathematical techniques not available for the particle sets. However this step can be done by a variety of methods some as simple as cloud-in-cell (CIC), or more complicated as smoothed-particle hydrodynamics (SPH), or using Voronoi and Delaunay tessellations as in the Delaunay Tessellation Field Estimator (DTFE) method ( van de Weygaert & Schaap 2009, Cautun et al. 2014). Recently a new method called a discrete persistent structure extractor (DisPerSE Sousbie 2011, Sousbie et al. 2011 allowing to identify haloes and other components of the web directly from the particles has been designed. This method can be applied to the galaxy catalogues, for instance Sousbie et al. (2011) applied it to SDSS catalogue and extracted the filaments (which are made available online).

An obvious advantage of methods based on particle coordinates, both based on the density field and directly on particle coordinates, is their applicability to redshift catalogues. The redshift catalogues like SDSS and 2dF provide only two angular coordinates and distances in redshift space. But cosmological N-body dark matter simulations provide the full dynamical information in six-dimensional phase space. This additional information is very valuable providing a greater opportunity for understanding the physics of the web and developing a better theory of the web.

Dark matter distribution in phase space is highly degenerate because it is cold. Practically, it occupies a three-dimensional sub-manifold in six-dimensional phase space. In the linear regime, the dark matter sub-manifold is a single-valued function of Eulerian coordinates which means that at each point the dark matter is represented by a single stream flow. As the density perturbations in dark matter grow with time the number of streams jumps to three at the regions of shell crossing. Then five stream regions emerge inside of the three stream regions and so on. Number of streams remains an odd integer in generic points. The corresponding parts of the three-dimensional dark matter sub-manifold form complicated folds in six-dimensional phase space.

The regions with multi-stream flow constitute the web while the regions with only one stream form voids (Shandarin 2011, Shandarin et al. 2012, Abel et al. 2012, Falck et al. 2012). This definition of voids states that in a given N-body simulation, no haloes can be formed before the first shell crossings have occurred and the smallest haloes cannot be smaller than the mass corresponding to the small scale cut-off in the initial power spectrum regardless of the cause of the cut-off: physical or due to numerical limitations (see e.g. Angulo et al. 2013). This definition of voids is physical by nature and thus has no free parameters. In addition, it does not speculate on the sub-grid physical processes. The first three-stream flow regions are similar to the pancakes in the ZA. They quickly grow and merge into a complicated three-dimensional structure; filaments making the framework of the web manifest themselves at the pancake crossings, and haloes emerge at the filament crossings. At later times different parts of the web participating in the large-scale motion overlap which increases the web complexity further.

Using the full six-dimensional information allows one to generate new fields which provide additional useful information about the evolution and morphology of the web. One of them is a multi-stream field in Eulerian space, which will be the focus of this paper. Another example is the flip-flop field in Lagrangian space. In cosmological context it was first used in the ZA. Vogelsberger & White (2011) used it in a study of multi-stream structure of galaxy size haloes. Shandarin & Medvedev (2014) applied it for identifying sub-haloes in dark matter haloes. A similar although somewhat simplistic realization of this idea has been revealed in the ORIGAMI method used for the analysis of the web ( Falck et al. 2012, Falck & Neyrinck 2015 ). Although these fields cannot be used directly on observational data because the full phase-space information is not available, they provide much deeper insight into non-linear clustering of collisionless dark matter and reveal new features of the web.

In order to compute the multi-stream field we will use the tessellation scheme described in Shandarin et al. (2012) which is also briefly discussed in Section 3. Using this methodology on the entire simulation box, we discuss the global behaviour of the number of streams in the cosmic web in Section 4. The tessellation technique we have utilized can be used to find multi-stream fields in smaller Eulerian boxes with very high resolution too. In Section 5 we study the local behaviour of multi-streams flows in regions around haloes the detected using friends-of-friends (FOF) technique.

## 2 THE SIMULATION

We have utilized the data from cosmological N-body simulations by Gadget-2 (Springel 2005) for 100 $h^{-1}$ Mpc and 200 $h^{-1}$ Mpc box sizes with $128^3$, $256^3$ and $512^3$ grids. Each particle is between $10^9 - 10^{12} M_\odot$. The initial conditions and cosmological parameters are consistent with the Planck cosmology. We utilize the initial Lagrangian box and do a three-dimensional mapping onto corresponding evolved simulations. In addition, for local multi-stream analyses around haloes, we have utilized halo catalogues for each of these simulation boxes. These haloes are detected using FOF method

considering objects with more than 20 particles found at linking length, $b = 0.2$.

## 3 MULTI-STREAM FIELD CALCULATION

Phase space tessellation considers the dynamics of the particles similar to that of a standard N-body code. However the particles are nodes of the tessellation, and are just massless tracers of the flow. Assuming that the uniform state is modelled by a simple rectangular grid, the particles are the nodes of the grid. Each elementary cube of the grid is tessellated by five tetrahedra (Shandarin et al. 2012[2]) of which the vertices are the vertices of the cube. Mass is assumed to be uniformly distributed within each tetrahedron and the tessellation remain intact at all times. The tetrahedra of the tessellation change their shapes and volumes, the latter are used for computing the densities of the tetrahedra. Despite the complicated deformations experienced by the three-dimensional sub-manifold tessellated by the tetrahedra, it remains continuous. Projected on three-dimensional configuration space, the tetrahedra may form complicated structures. The number of streams at a chosen point $\mathbf{x}$ is simply the number of tetrahedra that contain the point. The diagnostic points are computationally convenient to choose on a regular grid which can be significantly finer than the original grid in Lagrangian space. The ratio of separation of particles on the initial unperturbed grid to the separation distance of points in the diagnostic grid $l_{\rm part}/l_{\rm dg}$ will be referred to as the refinement factor in the rest of the paper.

Number of streams are odd-valued in the entire configuration space, except in a set of points of measure zero where caustics are formed. A single-stream flow implies that the tetrahedra do not overlap in the corresponding region and thus defined as a void region. The web is defined as a set of non-void regions, i.e. the set of regions where the number of stream is equal to or more than three. The level of non-linearity in the web can be quantitatively characterized by using 'number of streams' as a parameter. As shown in (Shandarin et al. 2012) there is no simple local relation between the number of streams and density, however the both fields are obviously correlated.

## 4 GLOBAL STATISTICS OF COSMIC WEB

The 3-dimensional multi-stream field for the entire simulation box exhibits cosmic web structure with void, walls, filaments and haloes. We propose the number of streams, '$n_{str}$' as a parameter for characterizing and distinguishing structures in the universe. This is different from Falck & Neyrinck (2015), where the authors have identified voids, walls, filaments and haloes by particles which have undergone any number of flip-flops along 0, 1, 2 or 3 axes respectively. Their description of voids is close to ours except that some particles that have experienced no flip-flops might be in the region of multi stream flow formed by other particles. Thus we expect that the mass fraction in voids defined as the regions with $n_{str} = 1$ is somewhat lower than that defined as the particles with flip-flops = 0 only at the final state. This is because some particles may have already fallen in the web but have not experienced flip flop yet and some particles that have experienced an even number of flip flops may come back to the original order. However the above arguments are valid only if the thickness of the web is the same in the both approaches. As we discuss below the thickness of the web in our analysis is about (100% - 84%)/(100%-93%)=2.3 times thinner than in the analysis by Falck & Neyrinck (2015) (See Table 4 for details). However Falck & Neyrinck (2015) discussed these effects and claimed that they were small.

Whereas for non-linear structures, our parameter space has more freedom in terms of number of streams. Similar to the density threshold, the number of streams - used as a local parameter - cannot distinguish unambiguously whether a point is in a wall, filament or halo. Only some parts of walls where there are only three streams can be identified locally without confusion. This is because the formation of a filament requires at least five streams. A flip-flop along one axis would produce a three-stream region which may be only a pancake. Therefore another flip-flop along the other axis in one of the streams from previous stage is required to transform it into a three-stream flow. Thus the total becomes five. However, if the second flip-flop happens along the same axis the resultant structure will remain a wall. Therefore some points in the five-stream flows can be within walls while the other in filaments. The present simulations have no information about the evolution of the flip-flop field therefore we rely on visual impressions initially to understand the transformation of walls into filaments and parts of filaments into haloes. By inspection, we have identified all the regions with three streams as walls. Unfortunately, walls are difficult to display on paper since they essentially block the view in two-dimensional projection. Nevertheless, we have demonstrated and analysed walls on a smaller Eulerian box around haloes in Section 5 using a simple and reasonably effective approximation.

For a multi-stream field calculated on a simulation box of size $100h^{-1}$ Mpc and $128^3$ particles, it is visually observed that with the increase of $n_{str}$ from 3 to 15, the corresponding occupied regions increasingly belong to filamentary structure rather than the membrane like walls, until at the level $n_{str} \gtrsim 17$ we observe that the number of wall points become negligible.

The filamentary structure of regions with 17 or more streams (denoted as 17+ ) is shown for a slice of simulation box of size $100h^{-1}$ Mpc and $128^3$ particles in Fig. 1. It has to be noted that all the regions with 17+ streams are regions with 3+ streams. Thus, the filaments are just interior parts of walls with higher $n_{str}$. These are visually observed mostly at the intersections of walls. Further, at the intersections of multiple filaments, there are regions with locally maximum number of streams, signifying the most dense regions in the simulations i.e. the dark matter haloes as Fig. 5 illustrates. By superimposing the positions from the FOF-halo catalogue, it is visually confirmed that the FOF haloes reasonably coincide with these high-streaming intersections, as Fig. 1 illustrates.

[2] For the description of an alternative type of the tessellation see Abel et al. (2012).

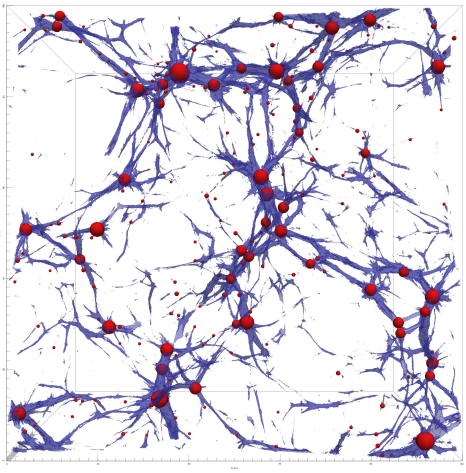

**Figure 1.** The cosmic web structure in a slice of $30h^{-1}$Mpc $\times$ $100h^{-1}$Mpc$\times 100h^{-1}$Mpc in a simulation box of size $100h^{-1}$ Mpc and $128^3$ particles. Regions with 17 or more streams (blue) form a filamentary structure. The haloes determined by FOF (red) are predominantly embedded in the intersections of the filaments.

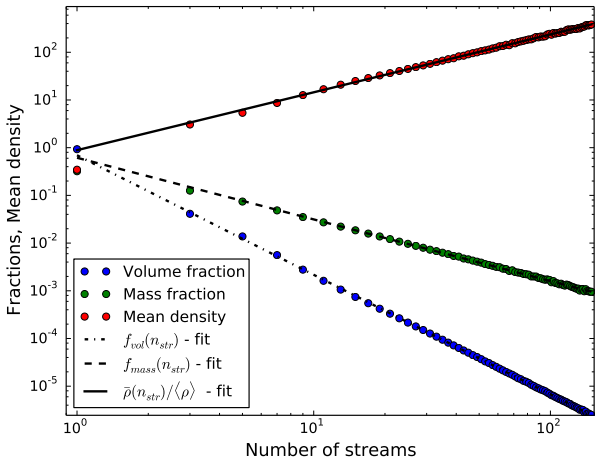


**Figure 2.** Volume and mass fraction of each stream, mean density of each stream in a box of size 100 $h^{-1}$ Mpc and $128^3$ particles. Exact values of fractions, density and their curve fit for the range $n_{str} \geqslant 5$ from Eq. 1, Eq. 2 and Eq. 3 are shown. Multi-streams are calculated with refinement factor of 8. The void ($n_{str} = 1$) occupies 93% of the volume and 55% of the mass.

### 4.1 Volume and mass fractions

The single-stream flow, which corresponds to the void, occupies majority of volume of the simulation box (Fig. 2). As mentioned in Section 4, higher multi-streaming flow regions are nested inside the lower streaming regions. Thus the volume occupied by higher number of streams monotonically decreases with the number of streams. This relation is approximately found to be a power law. For the box of size $L = 100$ $h^{-1}$ Mpc and $N = 128^3$ particles ($L/N = 0.78$ $h^{-1}$ Mpc), the volume fraction corresponding to each value of number of streams, $f_{vol}(n_{str})$ in the multi-stream field calculated with refinement factor of 8 (i.e. the multi-stream field was computed on $1024^3$ grid as described in Shandarin et al. (2012)) is

$$f_{vol}(n_{str}) = 0.69 n_{str}^{-2.5} \tag{1}$$

This is a good fit for the range of number of streams $n_{str} \geqslant 5$. In multi-stream field for the simulation box mentioned above, about 93% of the volume is occupied by 1-stream. With an increase in $n_{str}$, the corresponding volume fraction reduces. Physically, however, the number of streams reflect the advancement of non-linearity. Hence the higher $n_{str}$ regions are typically regions with higher densities. In effect, the mass fraction can also be approximated by a decreasing power law function of $n_{str}$,

$$f_{mass}(n_{str}) = 0.61 n_{str}^{-1.3} \tag{2}$$

This is also a good fit for the range of number of streams $n_{str} \geqslant 5$. For the same range of number of streams, the mean density in the regions with particular number of streams, given by the ratio of corresponding mass and volume fractions, increases as expected.

$$\frac{\bar{\rho}(n_{str})}{\langle\rho\rangle} = 0.89 n_{str}^{1.2}, \tag{3}$$

where $\langle\rho\rangle$ is the mean density of the universe. This also quantifies our previous claim that very high multi-streams correspond to the most dense areas in the Universe, i.e. the condensed haloes. The common over-density threshold of 200 using virial equilibrium corresponds to roughly 90 streams in Fig. 2 and Eq. 3.

Comparing the volume fractions of various simulation boxes in Fig. 3 and corresponding power law dependences in Table 1 (also, specifically for the volume fraction of voids in Table 2), we find that the profile is similar for boxes with same inter-particle resolution; i.e., equal box length to grid size ratio( For e.g., $L/N = 0.78$ $h^{-1}$ Mpc for the simulation box of 100 $h^{-1}$ Mpc - $128^3$ particles and 200 $h^{-1}$ Mpc - $256^3$ particles). The box with minimum inter-particle resolution in the data, hence the best raw resolution ( $L/N = 0.19$ $h^{-1}$ Mpc for 100 $h^{-1}$ Mpc, $512^3$ particles), has higher volume fraction for each multi-stream compared to lower resolution boxes. Additionally, it has a more non-linear stage advanced over time resulting from the initial small scale perturbations. The advancement of non-linearity manifests itself in higher number of streams. Box with the least raw inter-particle resolution ($L/N = 1.56$ $h^{-1}$ Mpc for 200 $h^{-1}$ Mpc, $128^3$ particles), occupies lower volumes than other boxes for each $n_{str}$. It is also prone to noise at very high streaming regions.

One of the advantages of using tessellation is the freedom to compute densities at very high resolutions (Abel et al. (2012), Shandarin et al. (2012)). We remind that the parameter 'refinement factor' denotes the ratio of separation of the particles to the separation distance of points in the diagnostic grid as defined in Sec. 3. High refinement factors are extensively used in understanding stream behaviour not only in the halo environment, but inside the halo too (Section 5). The volume fractions of resulting number of streams are similar for all refinement factors as shown in bottom of the Fig. 3 and in Table 3. Multi-stream fields calculated on low refinement factors are more noisy at high number of streams.

With same refinement factors, the mass fractions exhibit similar pattern for same $L/N$ as well (Fig. 4). The sim-

**Table 1.** Comparison of the approximate power law dependences of curve fits in Fig. 3 and Fig. 4. Power law relations for volume fraction $f_{vol}(n_{str})$ and mass fractions $f_{mass}(n_{str})$ as a function of number of streams at $n_{str} \geqslant 5$ are shown (amplitudes are not shown). The boxes of size 100 $h^{-1}$ Mpc on $128^3$ grids and, 200 $h^{-1}$ Mpc on $256^3$ grids have same $L/N = 0.78h^{-1}$ Mpc. Similarly, $L/N = 0.39h^{-1}$ Mpc for boxes of size 100 $h^{-1}$ Mpc on $256^3$ grids and, 200 $h^{-1}$ Mpc on $512^3$ grids.

| $L/N$ | 0.19 | 0.39 | 0.78 | 1.56 |
|---|---|---|---|---|
| $f_{vol}(n_{str})$ Vs. $n_{str}$ | $-2.1$ | $-2.3$ | $-2.5$ | $-2.9$ |
| $f_{mass}(n_{str})$ Vs. $n_{str}$ | $-1.1$ | $-1.2$ | $-1.4$ | $-2.0$ |

**Table 2.** Comparison of the volume and mass fractions of the void ($n_{str} = 1$) regions of the cosmic web for various simulation boxes at refinement factor of 1. Mean density is the ratio of mass fraction to the volume fraction. It is given in units of the mean density of the universe. The boxes of size 100 $h^{-1}$ Mpc on $128^3$ grids and, 200 $h^{-1}$ Mpc on $256^3$ grids have same $L/N = 0.78h^{-1}$ Mpc. Similarly, $L/N = 0.39h^{-1}$ Mpc for boxes of size 100 $h^{-1}$ Mpc on $256^3$ grids and, 200 $h^{-1}$ Mpc on $512^3$ grids.

| $L/N$ | 0.19 | 0.39 | 0.78 | 1.56 |
|---|---|---|---|---|
| Volume Fraction (%) | 88 | 90 | 93 | 96 |
| Mass Fraction (%) | 24 | 36 | 55 | 77 |
| Mean density | 0.27 | 0.40 | 0.59 | 0.80 |

ulation box with highest inter-particle distance (thus least mass resolution) has more mass particles in single streaming region, as tabulated in Table 2, but decreases steeply thereafter (Table 1). Unlike the volume fraction, the behaviour of mass fraction has a systematic variation across different refinement factors. The mass fractions given in Table 3 show that the single-streaming regions in the multi-stream fields with refinement factors 1 and 2 have higher mass fraction than in the fields with refinement factor of 8. Decreasing the resolution from refinement factor of 8 to 1 effectively introduces smoothing of the structure. This results in growth of mass fraction in voids ($n_{str} = 1$) and decreasing it in the web ($n_{str} > 1$). The multi-stream field is more robust as one can see in Fig. 3. and 4. In addition, the less refined multi-stream grids are prone to noise at high $n_{str}$ as usual.

**Table 3.** Comparison of the volume and mass fractions of the void ($n_{str} = 1$) regions of the cosmic web for a simulation box at different refinement factors. Mean density is the ratio of mass fraction to the volume fraction. All the multi-streams for simulation box of length 100 $h^{-1}$ Mpc on raw resolution of $128^3$ grids ($L/N = 0.78h^{-1}$)

| Refinement factor | 1 | 2 | 8 |
|---|---|---|---|
| Volume Fraction (%) | 93 | 93 | 93 |
| Mass Fraction (%) | 55 | 44 | 32 |
| Mean density | 0.59 | 0.47 | 0.35 |

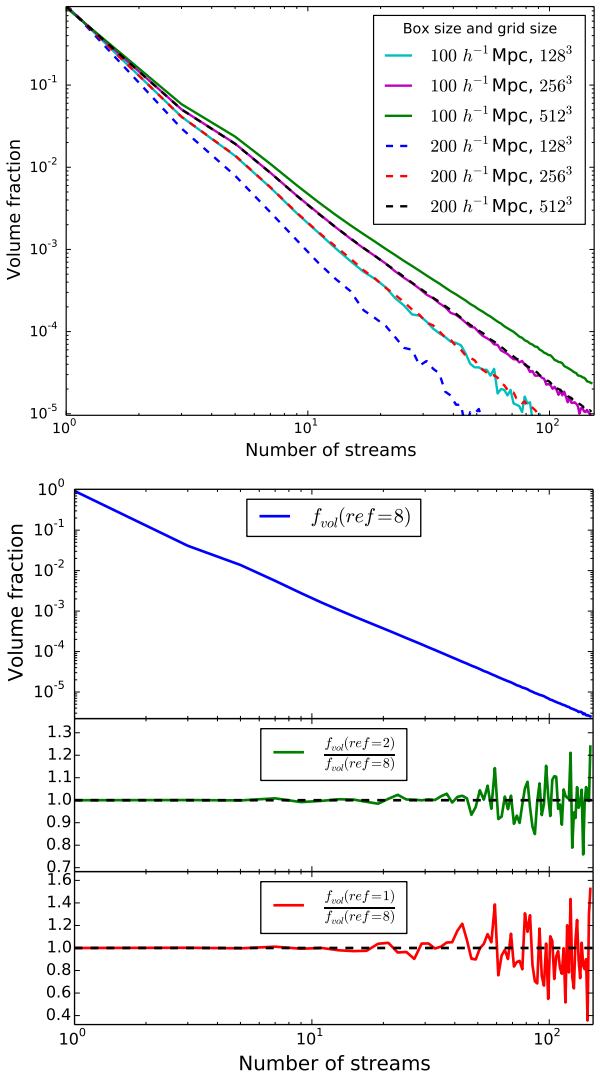


**Figure 3.** Top: Volume fraction distribution of streams in 6 simulation boxes of size 100 $h^{-1}$ Mpc, 200 $h^{-1}$ Mpc and $128^3$, $256^3$, $512^3$ grids (with refinement factor of 1). Volume fractions are similar for simulation boxes with same inter-particle resolution. Slopes of the curve fits are shown in Table 1. Bottom: Volume fraction distribution for different refinement factors for 100 $h^{-1}$ Mpc, $128^3$ box. A considerably smoother volume fraction distribution is obtained at high number of streams in multi-stream fields with high refinement factor.

## 5 STREAM ENVIRONMENT AROUND HALOES

Multi-stream field can be easily computed for a small Eulerian box with higher refinement factor. This can be utilized to analyse the phase-space behaviour inside and around haloes. In this section, we have used the halo coordinates identified by the FOF method, and selected Eulerian boxes around it. A reasonable correspondence between FOF halo centres and local maxima of multi-stream field is visually examined in Fig. 1.

Since each multi-stream region is surrounded by lower number of streams, the walls sandwich filaments within themselves (Fig. 5). The filaments are embedded with haloes at various intersections. These high-streaming haloes are

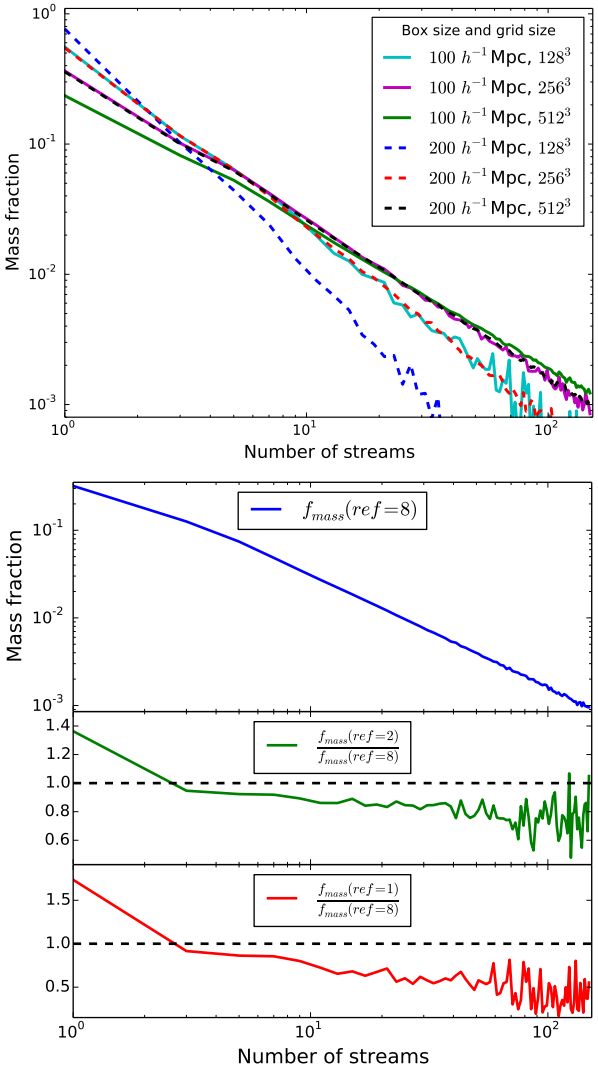


**Figure 4.** Top: Mass fraction distribution of streams in 6 simulation boxes of size 100 $h^{-1}$ Mpc, 200 $h^{-1}$ Mpc and $128^3$, $256^3$, $512^3$ grids ( with refinement factor of 1). Mass fractions are similar for simulation boxes with same inter-particle resolution. Slopes of the curve fits are shown in Table 1. Bottom: Mass fraction distribution for different refinement factors for 100 $h^{-1}$ Mpc, $128^3$ box. Single-streaming void regions have more fraction of mass particles in multi-stream fields calculated at low refinement factors of 1 and 2. This effect is minimized when calculation is done at better refinement. In addition, mass fraction distribution is less noisy.

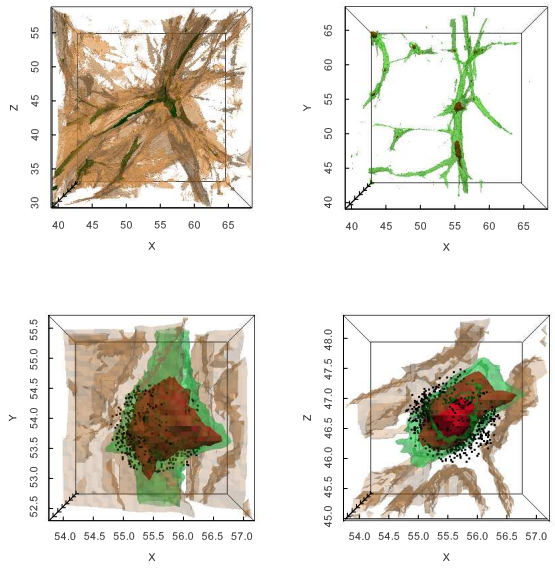


**Figure 5.** Multi-stream flow regions in a small box of the simulation. Top left: regions with more than 3-stream flow are identified as walls (brown). Intersection of multiple walls have higher $n_{str}$ regions (green, 17+ streams). Single-streaming voids (white) occupy large volume and are very close to the filaments in some directions. Top right: 17+ streams (green) form filamental structures with nodes at the intersections (red, 90+ streams) Bottom left and right: Closer look at the highly non-linear region reveals that a filament is sandwiched between the walls (brown). The 90+ stream region (red) forms a compact structure and is entirely contained within the filament. The black dots show the particles around the FOF halo within linking length of 0.2.

completely covered by relatively low-stream filaments and hence surrounded by walls too. This result differs considerably from the several void finder methods, which find existence of haloes within void regions (See Colberg et al. 2008 and references therein). By our classification, we distinguish configuration space of the simulation box as void and non-void or web regions. Further, we have made an attempt to classify the web into walls, filaments and haloes based on multi-stream thresholds. This classification based on number of stream threshold provides only a very crude description of visual impression from the richness, complexity and fundamentally multi-scale character of the web. The heuristic numbers we use in this paper are by no means universal, but may provide limited use in the discussion of these particular simulations.

Visual inspection of Fig. 5 reveals that the multi-stream environment of a halo is a highly intricate. Though the haloes are surrounded by filaments and walls, it can be surprisingly close to the voids in particular directions. Filaments defined by the multi-steam field are quite elongated, but the cross-sections are not circular or elliptical, and moreover, they branch-out and intersect at several regions. Finally, the haloes defined by contours of the multi-steam field look neither spherical nor ellipsoidal. We use a simple geometrical technique of projecting the number of streams onto a diagnostic spherical surface around a haloes to visualize and quantify their environments.

### 5.1 Technique

Motivated by the complicated morphology of multi-stream field around a dark matter halo, we devised an empirical statistical tool to quantify the multi-stream environment of the FOF haloes. The method is geometrical and non-local. We randomly select a large number of points on a diagnostic spherical surface centred at the FOF centre of the halo and compute the number of streams at these points. By increasing the radius of the sphere from inside of the halo to several times the halo radii, we estimate the fractions of the area on the diagnostic spherical surface occupied by the regions

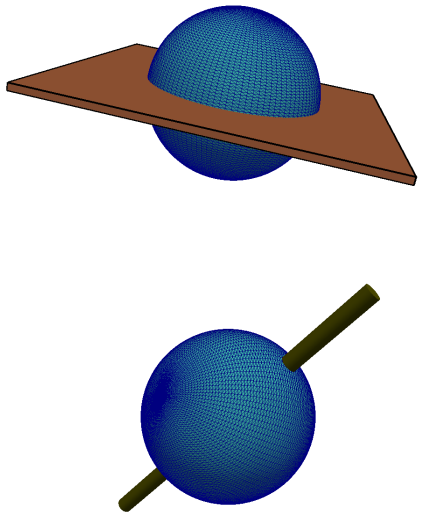

**Figure 6.** Modelling a wall and a filament. A diagnostic spherical surface is intersected by a cylinder and plane.

with different numbers of streams: 3+, 5+, ..., where $n$+ corresponds to $n$ or higher number of streams.

The geometry of a filament can be crudely approximated by a cylinder and that of a wall by a sheet with a small constant thickness 'd'. Upon intersecting with the spherical surface, these geometries occupy certain cross-sectional area, $Area_{c/s}$, on the sphere (See Fig. 6). The ratio of this area to the surface area of the sphere is given by,

$$f_{wall}(r) = \frac{Area_{c/s}}{4\pi r^2} = \frac{2\pi r d}{4\pi r^2} \propto r^{-1} \quad (4a)$$

$$f_{fil}(r) = \frac{Area_{c/s}}{4\pi r^2} = \frac{\text{const.}}{4\pi r^2} \propto r^{-2} \quad (4b)$$

The fractions of points on the surface of the sphere by multiple number of intersecting sheet-like walls or cylindrical filaments also scale proportional to $r^{-1}$ and $r^{-2}$ respectively.

For the diagnostic spheres of different radii, the scaling of multi-streams at the intersections is calculated. By checking the variation in the fraction of area occupied, we associate the number of streams with wall or halo.

Each of the Mollweide projections in Fig. 7 - 10 shows projection of the multi-stream field on to the spherical surface, and provide useful insight into the multi-stream structure around a halo. In a Mollweide projections, each filament stemmed from the halo looks as a compact patch. If the physical area of the cross section of the filament remains approximately constant, then the size of the patch on the Mollweide projection would decrease with the increasing radius of the diagnostic sphere. The cross section of a wall with the diagnostic sphere has a well known 'S'-shape (similar to the ecliptic plane in the galactic coordinates) and the width decreases with the growth of the diagnostic sphere. Both patterns are clearly seen in Fig. 7 - 10.

### 5.2 Voids, filaments and walls around haloes

From the technique described above, we arrive at quantitative thresholds for the different components of the web i.e., all regions where $n_{str} \geqslant 3$. We stress that this method is only a practical tool in arriving at heuristic thresholds of cosmic web structures. The analysis done here are for the simulation box of 100 $h^{-1}$ Mpc, $128^3$ particles, with refinement factor of 8.

The scaling of fraction of points with 3+ streams is closest to $r^{-1}$, where $r$ is the radius of the diagnostic sphere around the halo (Fig. 7 - 10; top figures). Since $r^{-1}$ variation is geometrically identical to that of a wall, it is identified as a flow region with 3+ stream flow. In this simulation the volume fraction of the web is dominated by 3-stream flows: $f_{vol}(3) \approx 0.04$ while $\sum_5^\infty f_{vol}(n_{str}) \approx 0.02$.

The deviation from the exact slope is expected, since assuming the filaments and walls as uniform cylinders and planes is rather crude. In the simulation, the filaments and walls have a far more complicated structure, where they branch out, and do not correspond to regular geometrical shapes. Detailed explanations for deviations are illustrated using Mollweide projections in the next section.

Variation of multi-streams regions of 5+ to 17+ streams steadily changes from $r^{-1}$ to $r^{-2}$. This smooth transition implies that finding an exact cut-off of $n_{str}$ for a filament is possible neither $n_{str}$ threshold nor by density. At 17+ stream regions scaling is closest to $r^{-2}$, the approximate filamentary geometry. In fact, $n_{str} = 19$+ regions also exhibit similar variation in spherical projections, but our choice of the threshold based on the lowest $n_{str}$ value that scales close to $r^{-2}$. Again, unlike the threshold for voids and walls, the threshold for filaments and haloes are not unambiguous. Our seemingly arbitrary choice of definition of filaments as regions with 17+ streams (in Section 4, Fig. 1 and Fig. 5) was motivated by this observation. Thus projections on a diagnostic sphere is a convenient tool for classifying regions in the simulation as belonging to void, wall, filament or a halo.

For illustrations, we have picked 4 haloes from different mass ranges: $3.7 \times 10^{14} M_\odot$, $5.0 \times 10^{13} M_\odot$ , $7.0 \times 10^{12} M_\odot$ and $1.1 \times 10^{12} M_\odot$ from the simulation box of 100 $h^{-1}$ Mpc length and $128^3$ particles. Multi-stream field with a high refinement factor of 8 is calculated for a greater resolution on scales of the halo volume. Diagnostic spheres of radii 0.1 $h^{-1}$ Mpc to 5 $h^{-1}$ Mpc are drawn for each of these haloes (Fig. 7 - 10; bottom figures), with the multi-stream field projected onto the surface. In the Mollweide projections of these spheres, the white space refers to single-stream voids. For the largest halo (Fig. 7) with FOF radii 1.2 $h^{-1}$ Mpc, the voids already appear in sphere of radius 1.5 $h^{-1}$ Mpc and in the smaller haloes (Fig. 10) it appears as early as 0.5 $h^{-1}$ Mpc.

Up to 1 $h^{-1}$ Mpc from halo center of the largest halo, the surfaces are uniformly covered with high number of streams (red, 17+). This shows that the most non-linear regions are close to centres of haloes. A similar trend is seen for the halo of radius 0.7 $h^{-1}$ Mpc (Fig. 8). However, for smaller haloes (Fig. 9 and 10) lower number of streams (even the wall forming 3+ streams; blue) start occupying the spherical surface at radii lesser than FOF-radius. In the case of the smallest halo of $1.1 \times 10^{12} M_\odot$ mass, the 17+ streams are seen at scales as low as 0.1 $h^{-1}$ Mpc. The distribution of multi-streams on the surface seems do not have a symmetry of any kind , signifying a complex morphology of the web in the vicinity of the haloes. Regions with 5+ to 15+ streams form structures intermediary to filament-like and wall-like

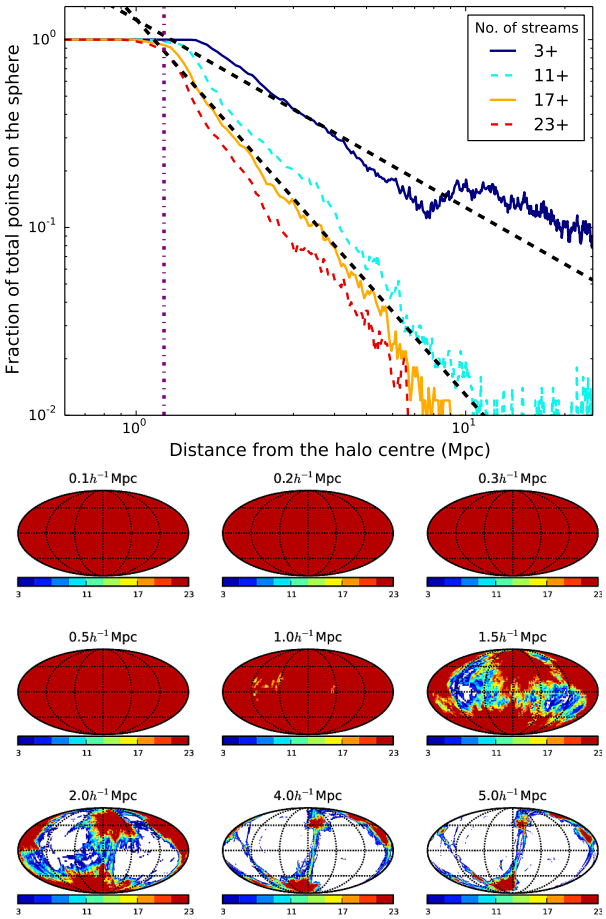


**Figure 7.** Large halo of mass $3.7 \times 10^{14} M_{\odot}$ and FOF radius 1.2 $h^{-1}$ Mpc (dotted-violet line in the top figure). Top: Fractional distribution of streams on the surface of spheres of increasing radii. Dashed-black lines are for $r^{-1}$ and $r^{-2}$ scaling. 3+ streams are closest to $r^{-1}$ and 17+ scales close to $r^{-2}$. for higher thresholds, the fractional distribution departs smoothly from $r^{-2}$. Bottom: Mollweide projection of multi-streams on the surface of the sphere.

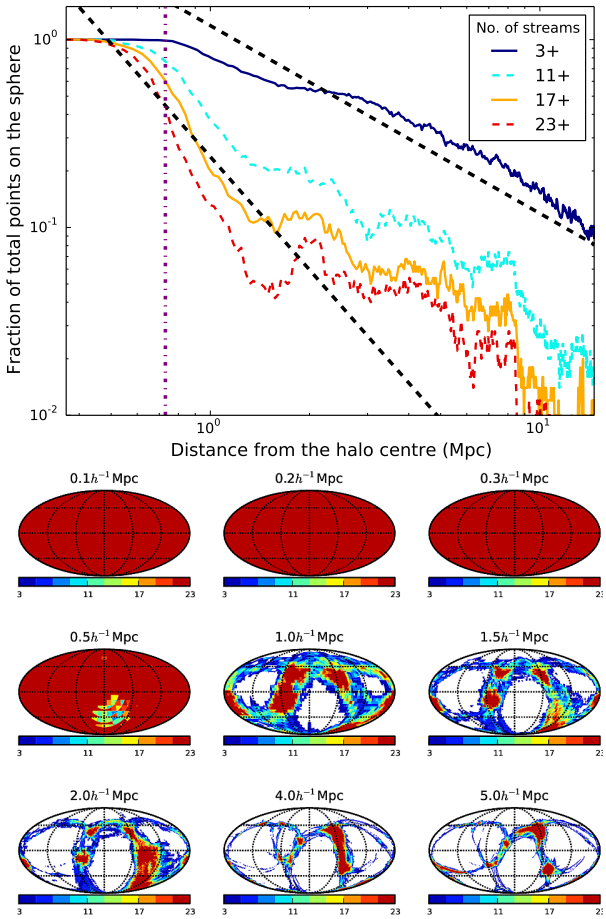


**Figure 8.** Halo of mass $5.0 \times 10^{13} M_{\odot}$ and FOF radius 0.7 $h^{-1}$ Mpc. Top: Fractional distribution of streams deviates from $r^{-1}$ and $r^{-2}$ scales since the high stream filament passes along the surface of the sphere. Bottom: Filament passing through the surface is seen from 2 to 5 times the halo radius.

behaviour, as seen by scaling of fraction of total points on the space with distance from halo center.

Halo environment at distance over twice the FOF radius reveals interesting morphological features. The walls intersect the sphere, and in the Mollweide projections, appear like a thin strip. We also note that a filament oriented tangentially to the diagnostic surface may occasionally appear as a strip too (like in Fig. 8, see the corresponding discrepancy in fraction of streams), but upon inspecting the spheres at various radii, we can clearly identify the persisting line-like structures, and they correspond to the walls. Similarly, a filament is projected as a compact patch structure, which occurs due to an intersection of a cylinder-like geometry with the spherical surfaces. It is clearly observed at the distance of 4 - 5 $h^{-1}$ Mpc in Fig. 7 and in between 0.5 - 5.0 $h^{-1}$ Mpc in Fig. 9.

Hence we conclude that the 3+ stream regions constitute predominantly walls and the regions with 17+ streams correspond mostly to filaments. The higher $n_{str}$ shells must be surrounded by the layers with lower $n_{str}$. Thus, the filaments are within the walls, and do not exist independently. We remind that the radius of diagnostic sphere varies from 0.1 - 5 $h^{-1}$ Mpc, whereas the Mollweide projections shown here are of the same size. Hence the walls and filaments appear more narrow and smaller in larger spheres due to zooming-out effects. In some cases (Fig. 8, 10), the Mollweide projections display the walls and filaments as a complicated network with patches of high number of streams.

The high peak shown by the curves corresponding to the numbers of streams from 11+ to 17+ in the top panel of Fig. 10 is mostly due to the presence of another halo nearby ( seen at bottom of Mollweide projection of 1 - 2 $h^{-1}$ Mpc). Fig. 8 also has a deviation from usual scaling, and this due to the intricate shape of 17+ stream filament, which appears to be branching out after 1 $h^{-1}$ Mpc.

Generally the transitions from haloes to filaments then to walls and finally to voids appear to be rather smooth. However occasionally sharp features as the one seen in Fig. 10 may emerge when the diagnostic sphere hits a neighbouring halo.

The friends-of-friends analysis identifies haloes as spherical structures. The distribution of multi-streams projected onto these surfaces of the FOF haloes can be utilized for a

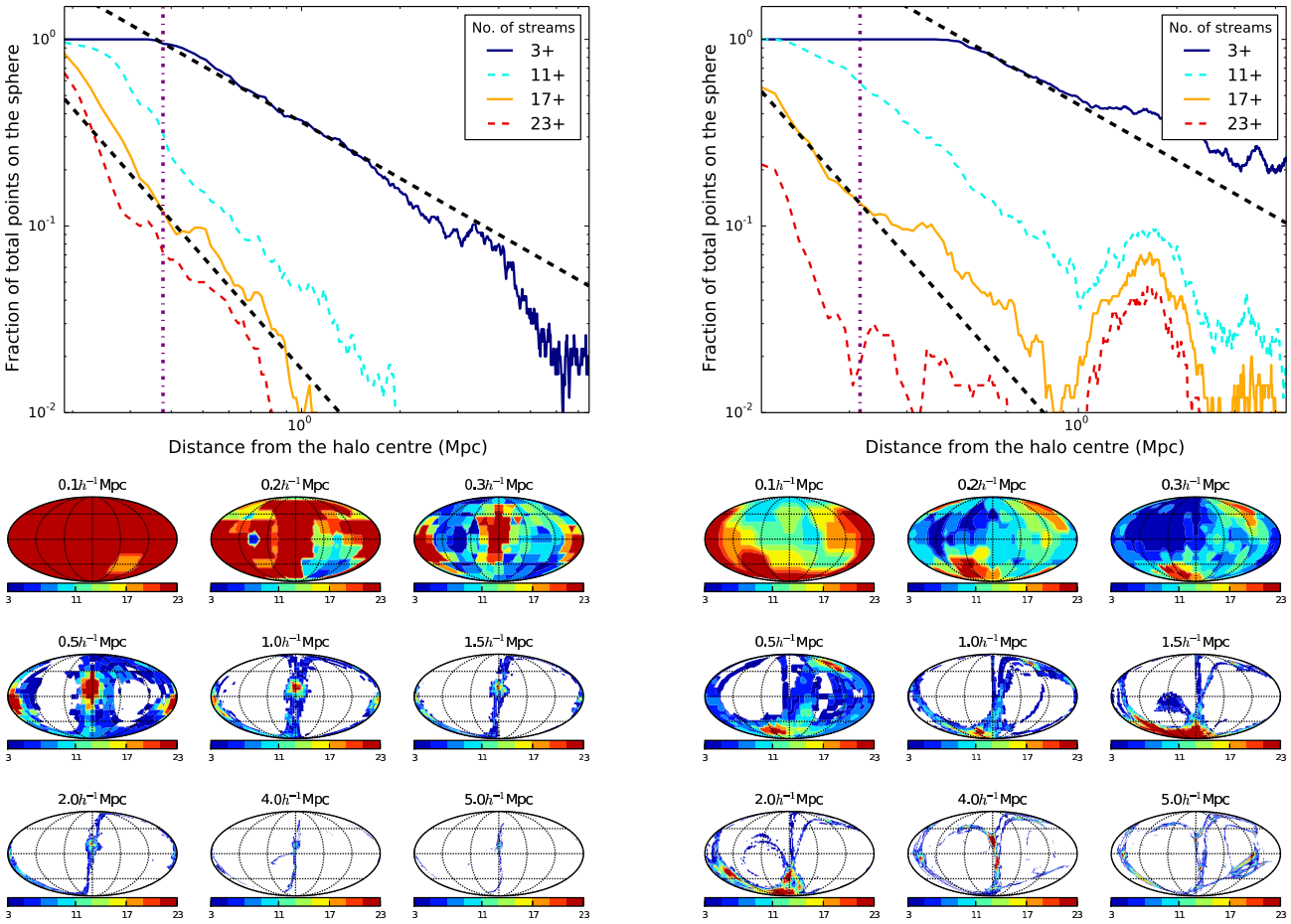


**Figure 9.** Halo of mass $7.0 \times 10^{12} M_{\odot}$ and FOF radius 0.4 $h^{-1}$ Mpc. Top: All lines clearly scale between $r^{-1}$ and $r^{-2}$. Bottom: The filament is passing through the centre. It persists from radius of halo to 4 $h^{-1}$ Mpc. It is also surrounded by a single wall appearing as a line in the middle.

statistical analysis of the haloes (Fig. 11 and 12). We have utilised FOF catalogues of haloes more than 20 particles found at linking length $b = 0.2$. The $n_{str}$ ranging from as low as 1 to higher than $10^3$ are seen on the halo surfaces. Haloes which have the minimum $n_{str} = 1$ are in contact with the void. However, if the maximum $n_{str}$ is also 1, then the halo is completely within the void. In calculations with low refinement factor of 1, only 7.3% (for $L/N = 0.78\,h^{-1}$) and 6.5% (for $L/N = 0.19\,h^{-1}$) of the haloes are completely within single streaming voids. This is solely due to low resolution of multi-stream field, since none of the FOF haloes are found in high resolution multi-stream calculations on both $L/N = 0.78\,h^{-1}$ and $L/N = 0.19\,h^{-1}$ boxes. At high refinement factors, none of the haloes are entirely embedded in a region with just one multi-stream value (i.e., $\max(n_{str}) = \min(n_{str})$, along the dotted-red lines in Fig. 11 and 12). However, there are significant number of haloes whose FOF surfaces are in contact with the void region: in calculations with refinement factor of 8, 62% of the haloes in $L/N = 0.78\,h^{-1}$ and 34% of the haloes in $L/N = 0.19\,h^{-1}$ are in contact with void on their FOF radii. Rest of the haloes are completely within non-void regions.

Statistical analysis of FOF haloes in Fig. 11 and 12

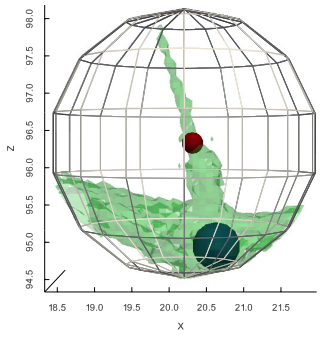


**Figure 10.** Halo of mass $1.1 \times 10^{12} M_{\odot}$ and FOF radius 0.2 $h^{-1}$ Mpc (dotted-violet line). This halo just has 26 particles, hence the resolution is lesser than previous haloes for surfaces with low radii. Top: There is a bump in fraction of each of 3+ streams a little over 1 $h^{-1}$ Mpc. This is due to the presence of an additional halo nearby, as seen in the projections. The Mollweide projections from 0.4 $h^{-1}$ Mpc to 2 $h^{-1}$ Mpc have high stream flow regions near the lower surfaces of diagnostic spheres. Bottom: Corresponding FOF halo (red, at the centre) has a more massive neighbouring FOF halo (blue) within distance of 2 $h^{-1}$ Mpc. The 17+ stream regions (green) are increased around the neighbouring halo.

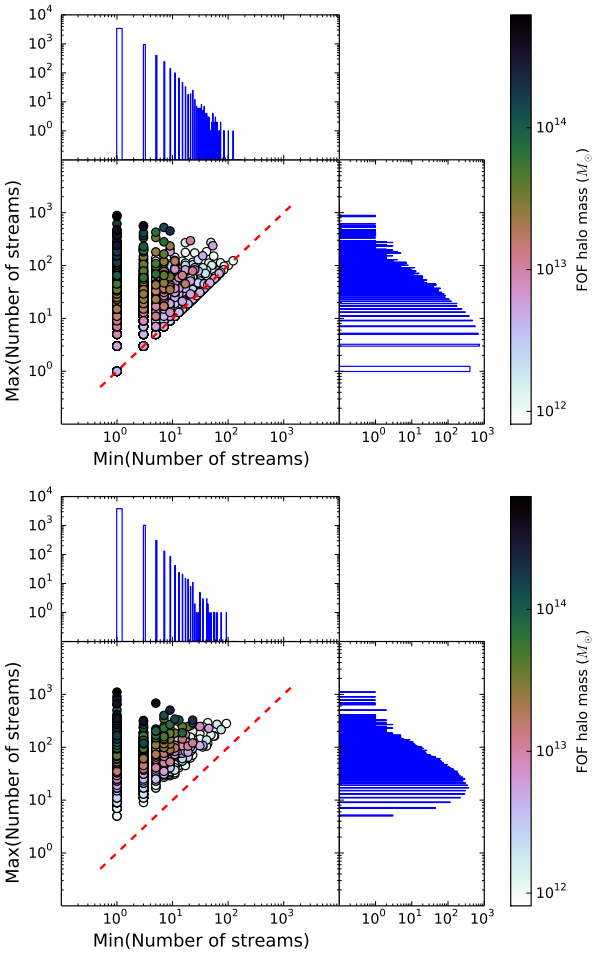


**Figure 11.** Scatter plot of minimum and maximum number of streams on the surface of FOF radius around all haloes in FOF catalogue. For the analysis, we use a total of 5521 haloes that are identified using the FOF technique with linking length, $b = 0.2$. Since several of the haloes coincide, distributions of number of haloes corresponding to minimum and maximum $n_{str}$ on their FOF radii are shown above and beside the scatter plot respectively. Top: Full box of $L = 100\ h^{-1}$ Mpc and $N = 128^3$ (i.e. $L/N = 0.78\,h^{-1}$), with a low refinement factor of 1 is utilized for multi-stream field calculation. Bottom: Same simulation box; multi-stream field calculated with higher refinement factor of 8.

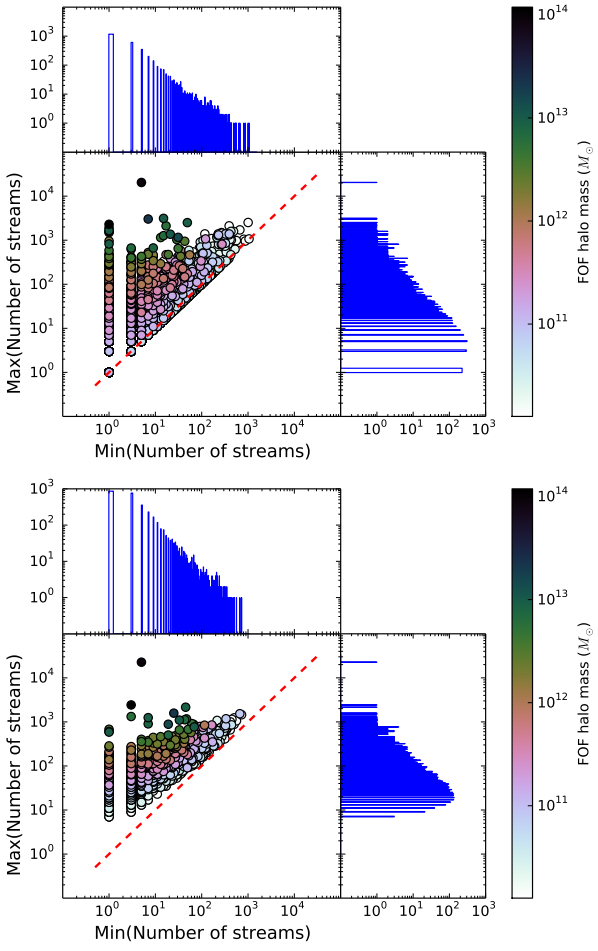


**Figure 12.** Scatter plot of minimum and maximum number of streams on the surface of FOF radius around all haloes in FOF catalogue. Distributions of number of haloes corresponding to minimum and maximum $n_{str}$ on their FOF radii are shown above and beside the scatter plot respectively. Top: In the simulation box of $L = 100\ h^{-1}$ Mpc and $N = 512^3$ (i.e. $L/N = 0.19\,h^{-1}$), multi-stream field is calculated on a smaller slice of 25 $h^{-1}$ Mpc is with a refinement factor of 1. Multi-stream field is projected onto surfaces of 3448 FOF haloes within this small box. Bottom: Same simulation box; the multi-stream field calculated on the the same small box, but with a refinement factor of 8.

show that massive haloes tend to have low $\min(n_{str})$ and high $\max(n_{str})$, hence a very diverse multi-stream environment on their spherical surface. The heuristic multi-stream threshold for haloes mentioned in Section 4 results in virialized haloes with a constant $n_{str}$ value. These halo surfaces far from sphere (see Fig. 5), whereas, the FOF surfaces are spherical and have a large range of number of streams on their surfaces. The probability distribution function of number of FOF haloes has an approximately exponential tail monotonically decreasing with with $\min(n_{str})$.

## 6 SUMMARY

In this paper, we explore for the first time, the multi-stream environment of dark matter haloes in cosmological N-body simulations. The visualization and quantitative characterization of generic non-linear fields in three-dimensional space represent a serious challenge from both conceptual and computational points of view. The complexity of the problem requires diverse tools for analysing the results of cosmological simulations as well as galaxy catalogues.

This study is different from the most previous works in a few aspects. Firstly, we consider the representation of the cosmic web in the form of a multi-stream field rather than a density field. The multi-stream field contains a different information about the web than the density and velocity fields and thus represents a complimentary characterization of the web revealing new dynamical features of the web (Shandarin 2011, Shandarin et al. 2012, Abel et al. 2012). Secondly, for computing the multi-stream field we use the tessellation of three-dimensional Lagrangian sub-manifold $\mathbf{x} = \mathbf{x}(\mathbf{q}, z = 0)$ in six-dimensional $(\mathbf{x}, \mathbf{q})$ space which allows to significantly increase the spatial resolution (Shandarin et al. 2012, Abel

et al. 2012). The Lagrangian sub-manifold is more convenient since $\mathbf{x}$ is a single-valued function of $\mathbf{q}$ at any stage including a highly non-linear regime while the phase space sheet projected on $\mathbf{x}$- or $\mathbf{v}$-space is not. If the initial state of the simulation is represented by a uniform three-dimensional mesh, then storing the Lagrangian sub-manifold does not require additional space for Lagrangian coordinates. And thirdly, in the study of the multi-stream environment of dark matter haloes we use the Mollweide projection of the multi-stream field computed on a set of diagnostic spherical surfaces centred at the FOF haloes and having radii from 0.1 $h^{-1}$Mpc to 5 $h^{-1}$Mpc.

Most of the results are obtained for a simulation in $L = 100h^{-1}$Mpc box with $N = 128$ particles along each axes although we report some of the results for the simulations in 100 $h^{-1}$Mpc box with $256^3$ and $512^3$ particles as well as in 200 $h^{-1}$Mpc box with $128^3$, $256^3$ and $512^3$ particles.

Using the tessellation of the three-dimensional Lagrangian sub-manifold $\mathbf{x} = \mathbf{x}(\mathbf{q}, t)$ (Shandarin et al. 2012), we compute the multi-stream field i.e. the number of streams on a regular grid in the configuration $\mathbf{x}$-space, $n_{str}(\mathbf{x})$ for estimating global parameters or on selected set of points in the study of the haloes environments.

The multi-stream field takes odd whole numbers everywhere except at a set of points of measure zero where it takes positive even whole numbers. This property is very useful for debugging the numerical code.

The multi-stream field allows one to define physical voids as the regions with $n_{str} = 1$. The rest of space with $n_{str} \geqslant 3$ can be called the non-void or web. This division of the space into two parts is unique and physically motivated: no object can form before shell crossing happens. It is worth emphasizing that the division of space into voids and web is based on the local parameter, the number of streams at a single point (Shandarin et al. 2012, Abel et al. 2012). Falck et al. (2012) and Falck & Neyrinck (2015) defined the web as a set of particles that experienced the 'flip-flop' at least once along any axis. We discussed potential problems with this definition in the beginning of Section 4.

The further division of the web into walls, filaments and haloes is not straightforward although haloes can be defined using dynamical parameters related to the requirement of virialization of haloes. One of the simplest is the famous density threshold $\rho/\bar{\rho} \approx 200$. Identifying filaments and walls is significantly more tricky (see e.g. Hahn et al. 2007, Forero-Romero et al. 2009, Aragón-Calvo et al. 2010, Cautun et al. 2014, Falck & Neyrinck 2015) and require non-local parameters.

The large part of walls can also be identified locally since the regions where $n_{str} = 3$ can be neither filaments nor haloes. For instance, in the simulation 100 $h^{-1}$Mpc box with $128^3$ particles the web occupies about 6% of the volume, the three-stream flow regions occupy about 4% and the rest of the web remaining 2% of the total volume.

In this study we introduced an empirical statistical criteria which very crudely distinguish wall, filament and haloes. We have found empirically that in the studied simulation the transition from wall points to filament points takes place approximately at $5 \leqslant n_{str} \lesssim 15$. Using the virial over-density threshold of 200 in Eq. 3, we have also estimated that the haloes correspond to the regions with $n_{str} \gtrsim 90$. Thus, the transition from filament to haloes takes place in the range $17 \leqslant n_{str} \lesssim 90$. The above critical values for transition from walls to filaments and from filaments to haloes were shown to be approximately correct for the simulation with $L/N = 0.78h^{-1}$ Mpc. This technique can be also applied to simulations with different $L/N$ ratio and multi-stream grid of different refinement factors but the classification based on the threshold applied locally will remain only a very crude estimator. A more sophisticated morphological analysis will require non-local geometric and topological methods, which is beyond the scope of this paper.

We have found that the volume and mass fractions in the voids are approximately V.F./M.F. = 96/76, 93/32 and 88/24, where each number is the percentage, for the simulations with $L/N = 1.56\,h^{-1}$, $0.78\,h^{-1}$ and $0.19\,h^{-1}$ Mpc respectively. As the ratio $L/N$ gets smaller both volume and mass fractions in voids monotonically decrease. This is fairly consistent with the results of Falck & Neyrinck (2015), considering the differences between our numerical methods. We compare the fractions of the volumes and masses in other components of the web in Table 4, and the results are in a good qualitative agreement. Our estimates systematically higher for both volume and mass fractions for voids and thus systematically lower for the web. One general conclusion seems to be obvious: the web defined by the multi-stream flows is about (100% - 84%)/(100%-93%)=2.3 times thinner than that defined by the ORIGAMI method.

In conclusion we would like to outline the major aspects of the web revealed by the study of the multi-stream field. The multi-stream field is a fundamental attribute of the structures formed in cold collision-less dark matter. Its properties are of great importance for the detecting dark matter directly in a laboratory setting or indirectly via astronomical observations. The dark matter web described by a multi-stream field represents a nested structure, consisting of layers with increasing number of streams. The number of streams are odd integers almost everywhere except on caustics where they are even integers. The caustics occupy infinitesimal volume. The most of the volume is occupied by one stream flow regions which are dark matter voids. The regions with three streams are the regions occupying the second largest volume. They form very thin membrane type structures (often referred to as walls or pancakes) most of which are connected in one huge connected formation. The three-stream regions form the external shell of the web. All other structures filaments and haloes are within the three-stream shell. The membranes are attached to each others by the filaments which locally consist of regions with higher number of streams than the neighbouring membranes. The filaments form the framework or a skeleton of the dark matter web. Similar to a real skeleton, the filamental structure has joints where most of the the dark matter haloes are located. The haloes are the local peaks of the multi-stream field.

## ACKNOWLEDGEMENTS

The authors are grateful to Gustavo Yepes and Noam Libeskind for providing the simulations used in this study and the Sir John Templeton Foundation for the support.The authors would also like to thank the anonymous referee for careful review and useful suggestions.

**Table 4.** Comparison of the volume and mass fraction of the elements of the cosmic web between our analysis and Falck & Neyrinck (2015). $L/N = 0.78h^{-1}$ Mpc for simulations used in both techniques. We use a refinement factor of 8 for the multi-stream grid. The mean density is given in units of the mean density of the universe.

| | Multi-stream analysis (This work) | | | | ORIGAMI (Falck & Neyrinck 2015) | | | |
|---|---|---|---|---|---|---|---|---|
| | Voids | Walls | Filaments | Haloes | Voids | Walls | Filaments | Haloes |
| Volume Fraction (%) | 93 | 7 | $< 1$ | $< 0.1$ | 84 | 12 | 3 | $< 1$ |
| Mass Fraction (%) | 32 | 35 | 17 | 14 | 26 | 19 | 19 | 35 |
| Mean density | 0.34 | 5 | $> 17$ | $> 140$ | 0.31 | 2.2 | 6 | $> 35$ |

## REFERENCES


Abel T., Hahn O., Kaehler R., 2012, MNRAS, 427, 61
Angulo R. E., Hahn O., Abel T., 2013, MNRAS, 434, 3337
Aragón-Calvo M. A., van de Weygaert R., Jones B. J. T., 2010, MNRAS, 408, 2163
Arnold V. I., Shandarin S. F., Zeldovich Y. B., 1982, Geophysical and Astrophysical Fluid Dynamics, 20, 111
Bond J. R., Kofman L., Pogosyan D., 1996, Nature, 380, 603
Cautun M., van de Weygaert R., Jones B. J. T., Frenk C. S., 2014, MNRAS, 441, 2923
Colberg J. M., et al., 2008, MNRAS, 387, 933
Elahi P. J., et al., 2013, MNRAS, 433, 1537
Falck B., Neyrinck M. C., 2015, MNRAS, 450, 3239
Falck B. L., Neyrinck M. C., Szalay A. S., 2012, ApJ, 754, 126
Forero-Romero J. E., Hoffman Y., Gottlöber S., Klypin A., Yepes G., 2009, MNRAS, 396, 1815
Frenk C. S., White S. D. M., Davis M., 1983, ApJ, 271, 417
Hahn O., Carollo C. M., Porciani C., Dekel A., 2007, MNRAS, 381, 41
Hoffmann K., et al., 2014, MNRAS, 442, 1197
Klypin A. A., Shandarin S. F., 1983, MNRAS, 204, 891
Knebe A., et al., 2013, MNRAS, 435, 1618
Oort J. H., 1983, Annual Review of Astronomy as Astrophysics, 21, 373
Shandarin S. F., 2011, Journal of Cosmology as Astroparticle Physics, 5, 15
Shandarin S. F., Klypin A. A., 1984, Soviet Astronomy, 28, 491
Shandarin S. F., Medvedev M. V., 2014, preprint, (`arXiv:1409.7634`)
Shandarin S., Zeldovich Y., 1989, Rev. Mod. Phys., 61, 185
Shandarin S., Habib S., Heitmann K., 2012, Phys. Rev. D, 85, 083005
Sousbie T., 2011, MNRAS, 414, 350
Sousbie T., Pichon C., Kawahara H., 2011, MNRAS, 414, 384
Springel V., 2005, MNRAS, 364, 1105
Vogelsberger M., White S. D. M., 2011, MNRAS, 413, 1419
Zel'dovich Y. B., 1970, A&A, 5, 84
van de Weygaert R., Schaap W., 2009, in Martínez V. J., Saar E., Martínez-González E., Pons-Bordería M.-J., eds, Lecture Notes in Physics, Vol. 665, Data Analysis in Cosmology. Berlin Springer Verlag, pp 291–413, doi:10.1007/978-3-540-44767-2˙11